PERGAMON

International Journal of Heat and Mass Transfer 45 (2002) 785–792

International Journal of HEAT and MASS TRANSFER

www.elsevier.com/locate/ijhmt

Numerical computations of Factor Xa and thrombin productions using a finite-volume method

John C. Chai *, T.M. Tsai, Ji Jinn Foo, Vincent Chan

School of Mechanical and Production Engineering, Nanyang Technological University, Nanyang Avenue, Singapore 639798, Singapore

Received 3 April 2001; received in revised form 31 May 2001

Abstract

The formations of Factor Xa and thrombin, two intermediate chemicals leading to the formation of blood clots in damaged blood vessels are predicted in this paper using a finite-volume method. The steady-state forms of the continuity, momentum and concentration equations are solved. The surface reactions are modeled using the classical Michaelis–Menten reaction kinetics. The results are compared with three sets of experimental data. These experiments were conducted using circular tubes and parallel flat plates. The present computational model is able to predict experimental results very well over a range of shear rates and inlet concentrations.

1. Introduction

The aggregation of platelets in damaged blood vessels forms blood clots. This leads to the formation of insoluble fibrin network, which further traps blood cells. Fibrin is the product of a complex chain of reactions, which involves both enzymes and nonenzymatic cofactors [1]. Two of these reactions are the formation of Factor Xa from Factor X and the formation of thrombin from prothrombin.

Experimental results on the formation of thrombin were reported by Billy et al. [2]. The average thrombin flux was presented for two shear rates and various inlet prothrombin concentrations. Two different tube diameters were used in the above experiments. Gemmell et al. [3] and Hall et al. [4] reported experimental data on the formation of Factor Xa. Numerical simulations of the above experiments were conducted by Gir et al. [5] and Hall et al. [6]. Gemmell et al.'s experiments were carried out using circular tubes, while Hall et al., measured the formation of Factor Xa using two parallel plates. In the numerical studies conducted in [5,6], the classical Michaelis–Menten reaction kinetics were used to model the surface reactions. Hall et al. [6] used a commercial software package to model the experiments.

The objective of this paper is to present a numerical study on the prediction of the formations of thrombin and Factor Xa using a finite-volume method [7]. The surface reactions are modeled using the Michaelis–Menten reaction kinetics.

The remainder of this paper is divided into three sections. The governing equations, boundary conditions, average flux and numerical procedure employed are discussed in the next section. This is followed by the presentation of the results and the associated discussion for three experiments. Finally, some concluding remarks are given to conclude the paper.

2. Governing equations and boundary conditions

2.1. Governing equations

The continuity, momentum and concentration equations can be written as

Continuity

$$\frac{\partial(\rho u)}{\partial x}+\frac{1}{r^a}\frac{\partial(\rho r^a v)}{\partial r}=0. \tag{1}$$

* Corresponding author. Tel.: +65-790-4270; fax: +65-792-4062.

E-mail address: mckchai@ntu.edu.sg (J.C. Chai).

0017-9310/02/$ - see front matter
PII: S0017-9310(01)00197-1

Nomenclature

a	coordinate indicator
c	concentration of prothrombin or Factor X
c_{in}	inlet concentration of prothrombin or Factor X
C	dimensionless concentration of prothrombin or Factor X
D	depth of the channel
D_s	diffusion coefficient of prothrombin or Factor X
H	height of channel
k_m	Michaelis constant
K_m	dimensionless k_m
l_y	length scale in the transverse direction
p	pressure
P	dimensionless pressure
Pe	Peclet number
Re	Reynolds number
q_c	boundary prothrombin or Factor X flux
Q	volumetric flow rate
Q_c	dimensionless q_c
r_0	radius of the tube
u, v	dimensional axial and transverse velocities
u_{max}	maximum axial velocity
U, V	dimensionless axial and transverse velocities
u_{in}	inlet axial velocity
w_{max}	maximal conversion rate per unit area
W_{max}	dimensionless w_{max}
x, y, r	coordinates
X, Y, R	dimensionless coordinates

Greek symbols

γ	shear rate
ρ	density
μ	viscosity

Subscripts

ave	average
in	inlet
max	maximum

Axial momentum

$$\rho u\frac{\partial u}{\partial x}+\rho v\frac{\partial u}{\partial r}=\frac{\partial}{\partial x}\left(\mu\frac{\partial u}{\partial x}\right)+\frac{1}{r^a}\frac{\partial}{\partial r}\left(\mu r^a\frac{\partial u}{\partial r}\right)-\frac{\partial p}{\partial x}. \quad (2)$$

Transverse momentum

$$\rho u\frac{\partial v}{\partial x}+\rho v\frac{\partial v}{\partial r}=\frac{\partial}{\partial x}\left(\mu\frac{\partial v}{\partial x}\right)+\frac{1}{r^a}\frac{\partial}{\partial r}\left(\mu r^a\frac{\partial v}{\partial r}\right)-\frac{\partial p}{\partial r}-a\frac{\mu v}{r^2}. \quad (3)$$

Concentration

$$u\frac{\partial c}{\partial x}+v\frac{\partial c}{\partial r}=\frac{\partial}{\partial x}\left(D_s\frac{\partial c}{\partial x}\right)+\frac{1}{r^a}\frac{\partial}{\partial r}\left(D_s r^a\frac{\partial c}{\partial r}\right). \quad (4)$$

In Eqs. (1)–(4), x and r are the axial and the transverse coordinates, respectively. The symbol a is set to zero for Cartesian coordinates and one for axisymmetric computations. The above equations can be non-dimensionalized as

Continuity

$$\frac{\partial U}{\partial X}+\frac{1}{R^a}\frac{\partial(R^aV)}{\partial R}=0. \quad (5)$$

Axial momentum

$$U\frac{\partial U}{\partial X}+V\frac{\partial U}{\partial R}=\frac{1}{Re}\frac{\partial}{\partial X}\left(\frac{\partial U}{\partial X}\right)+\frac{1}{Re}\frac{1}{R^a}\times\frac{\partial}{\partial R}\left(R^a\frac{\partial U}{\partial R}\right)-\frac{\partial P}{\partial X}. \quad (6)$$

Transverse momentum

$$U\frac{\partial V}{\partial X}+V\frac{\partial V}{\partial R}=\frac{1}{Re}\frac{\partial}{\partial X}\left(\frac{\partial V}{\partial X}\right)+\frac{1}{Re}\frac{1}{R^a}\times\frac{\partial}{\partial R}\left(R^a\frac{\partial V}{\partial R}\right)-\frac{\partial P}{\partial R}-a\frac{1}{Re}\frac{V}{R^2}. \quad (7)$$

Concentration

$$U\frac{\partial C}{\partial X}+V\frac{\partial C}{\partial R}=\frac{1}{Pe}\frac{\partial}{\partial X}\left(\frac{\partial C}{\partial X}\right)+\frac{1}{Pe}\frac{1}{R^a}\times\frac{\partial}{\partial R}\left(R^a\frac{\partial C}{\partial R}\right) \quad (8)$$

using the following dimensionless variables:

$$X=\frac{x}{l_y},\quad R=\frac{r}{l_y}, \quad (9a)$$

$$U=\frac{u}{u_{in}},\quad V=\frac{v}{u_{in}}, \quad (9b)$$

$$P=\frac{p}{\rho u_{in}^2},\quad C=\frac{c}{c_{in}}, \quad (9c)$$

$$Re=\frac{\rho u_{in}l_y}{\mu},\quad Pe=\frac{u_{in}l_y}{D_s}. \quad (9d)$$

The characteristic lengths l_y are the radius of the tube r_0 and the height of the channel H for the axisymmetric and the parallel plate geometries respectively. The meanings of various variables used in Eqs. (9a)–(9d) are defined in the nomenclature. All properties are assumed constant in this paper. From Eqs. (5)–(8), it is clear that the solutions depends on the Reynolds number Re, and the Peclet number Pe. The boundary conditions for the two geometries are presented next.

2.2. Boundary conditions

Fig. 1 shows the schematics of the computational domains. The following are used as the boundary conditions in this paper:

Axisymmetric flow

$$\text{Inlet } (x=0) \qquad u=u_{\text{in}}, \quad v=0, \quad c=c_{\text{in}}, \tag{10a}$$

$$\text{Outlet } (x=x_{\max}) \qquad \frac{\partial v}{\partial x}=0, \quad \frac{\partial c}{\partial x}=0, \tag{10b}$$

$$\text{Bottom } (r=0) \qquad \frac{\partial u}{\partial r}=0, \quad v=0, \quad \frac{\partial c}{\partial r}=0, \tag{10c}$$

$$\text{Top } (r=r_0) \qquad u=0, \quad v=0, \quad q_c=-w_{\max}\frac{c}{c+k_{\text{m}}}. \tag{10d}$$

Parallel plate flow

$$\text{Inlet } (x=0) \qquad u=u_{\text{in}}, \quad v=0, \quad c=c_{\text{in}}, \tag{11a}$$

$$\text{Outlet } (x=x_{\max}) \qquad \frac{\partial v}{\partial x}=0, \quad \frac{\partial c}{\partial x}=0, \tag{11b}$$

$$\text{Bottom } (y=0) \qquad u=0, \quad v=0, \quad \frac{\partial c}{\partial y}=0, \tag{11c}$$

$$\text{Top } (y=H) \qquad u=0, \quad v=0, \quad q_c=-w_{\max}\frac{c}{c+k_{\text{m}}}. \tag{11d}$$

The axial velocities at the exits ($x=x_{\max}$) are calculated to ensure mass conservation. The dimensionless forms of the boundary conditions are:

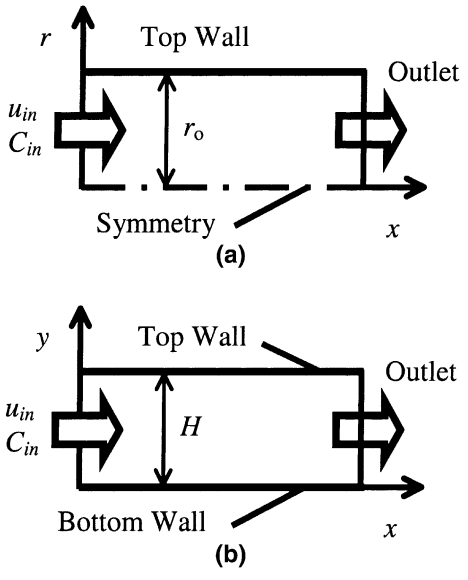

Fig. 1. Schematics of experiments: (a) axisymmetric, (b) parallel plates.

Axisymmetric flow

$$\text{Inlet } (X=0) \qquad U=1, \quad V=0, \quad C=1, \tag{12a}$$

$$\text{Outlet } (X=X_{\max}) \qquad \frac{\partial V}{\partial X}=0, \quad \frac{\partial C}{\partial X}=0, \tag{12b}$$

$$\text{Bottom } (R=0) \qquad \frac{\partial U}{\partial R}=0, \quad V=0, \quad \frac{\partial C}{\partial R}=0, \tag{12c}$$

$$\text{Top } (R=1) \qquad U=0, \quad V=0, \quad Q_c=-W_{\max}\frac{C}{C+K_{\text{m}}}. \tag{12d}$$

Parallel plate flow

$$\text{Inlet } (X=0) \qquad U=1, \quad V=0, \quad C=1, \tag{13a}$$

$$\text{Outlet } (X=X_{\max}) \qquad \frac{\partial V}{\partial X}=0, \quad \frac{\partial C}{\partial X}=0, \tag{13b}$$

$$\text{Bottom } (Y=0) \qquad U=0, \quad V=0, \quad \frac{\partial C}{\partial Y}=0, \tag{13c}$$

$$\text{Top } (Y=1) \qquad U=0, \quad V=0, \quad Q_c=-W_{\max}\frac{C}{C+K_{\text{m}}}. \tag{13d}$$

The axial velocities at the exits ($X=X_{\max}$) are calculated to ensure mass conservation. Most dimensionless variables are defined in Eqs. (9a)–(9d). Additional dimensionless variables used in the above equations are

$$K_{\text{m}}=\frac{k_{\text{m}}}{c_{\text{in}}}, \quad W_{\max}=\frac{w_{\max}l_y}{D_{\text{s}}c_{\text{in}}}, \quad Q_c=\frac{l_y q_c}{D_{\text{s}}c_{\text{in}}}. \tag{14}$$

2.3. Developing and fully developed velocity fields

When the flow is assumed to be fully developed, the solutions of the continuity, axial momentum and transverse momentum equations yield the following relations:

Axisymmetric flow

$$u=2u_{\text{in}}\left[1-\left(\frac{r}{r_0}\right)^2\right], \tag{15a}$$

$$u_{\max}=2u_{\text{in}}, \tag{15b}$$

$$\gamma=\frac{4Q}{\pi r_0^3}. \tag{15c}$$

Parallel plate flow

$$u=6u_{\text{in}}\left[\frac{y}{H}-\left(\frac{y}{H}\right)^2\right], \tag{16a}$$

$$u_{\max}=\frac{3}{2}u_{\text{in}}, \tag{16b}$$

$$\gamma = \frac{6Q}{DH^2}. \tag{16c}$$

The concentration (Eq. (4) or Eq. (8)) is solved using the fully developed velocity profiles given in Eq. (15a) or (16a). When fully developed flow is assumed, the solution of the concentration equation requires the specifications of u_{in}, D_s, k_m and w_{max}.

When the velocity boundary layer is allowed to develop, the continuity, axial momentum and transverse momentum equations (Eqs. (1)–(3) or Eqs. (5)–(7)) are solved to obtain the velocity distributions inside the solution domains. Once the velocity distribution is obtained, the concentration equation (Eq. (4) or Eq. (8)) is solved to obtain the concentration profile.

2.4. Average flux

Once the concentration distribution is obtained, the average flux is calculated using the following relation:

$$q_{ave} = \frac{\int_{x=0}^{x=x_{max}} q_c|_{r=l_y}\,dx}{x_{max}}. \tag{17}$$

The equation is valid for both axisymmetric and parallel plate geometries using the l_y appropriate to the specific geometry.

2.5. Numerical procedure

When the flow is allowed to develop, the continuity and the momentum equations given in Eqs. (1)–(3) or Eqs. (5)–(7) are solved. The concentration given by Eq. (4) or Eq. (8) is then solved to obtain thrombin flux or Factor Xa flux. When flow field is assumed to be fully developed, the velocity profiles given by Eq. (15a) or Eq. (16a) are specified and the concentration given by Eq. (4) or Eq. (8) is then solved to obtain thrombin flux or Factor Xa flux. In both cases, the velocity field is decoupled from the concentration field. The governing equations for mass, momentum and concentration are solved using the finite-volume approach described by Patankar [7]. When needed, the SIMPLER algorithm of Patankar [7] is used to resolve the pressure–velocity coupling. A block-correction procedure is used to enhance convergence.

3. Results and discussions

Three different sets of results are presented in this section. The results are compared with available experimental data reported by Billy et al. [2], Gemmell et al. [3] and Hall et al. [4]. These results show that the present computational model produces accurate solutions for the production of Factor Xa from Factor X and the production of thrombin from prothrombin using the Michaelis–Menten kinetics. The first two problems consist of flow inside axisymmetric tubes, while the third problem is for flow between two parallel plates.

3.1. Problem 1

3.1.1. Problem description

The experiment was presented by Billy et al. [2]. It consists of flow inside a circular tube. Four different sets of experiments were carried out using two different volumetric flow rates and two tube radii. Since experimental values are presented for two sets of experiments, these cases are simulated and presented. The length of the tube was kept at 12.7 cm for all cases. The important parameters are summarized in Table 1. As discussed earlier, both the density ρ, and viscosity μ, are needed in the solution of the momentum and continuity equations when the flow is allowed to develop. These values are taken as $\rho = 1.028$ g/cm^3 and $\mu = 0.012$ g/(s cm), respectively. The diffusion coefficient of prothrombin is $D_s = 1 \times 10^{-6}$ cm^2/s. The Reynolds and Peclet numbers are defined in Eq. (9d). The schematic of the problem is shown in Fig. 1(a).

3.1.2. Discussions of results

The effects of spatial grid resolutions are examined. Fig. 2 shows the average thrombin production rate calculated from Eq. (17) using values of parameters shown in case 2 with two spatial grids. First, the computation is carried out using a "coarse" grid of 40×200 control volumes in the radial and axial directions, respectively. The number of control volumes in each direction are then increased to 80×400 control volumes. The predicted thrombin production rate (Fig. 2) shows that the solution does not change with spatial grid (identical) or the grid independent solution has been obtained. As a result, the coarser grids of 40×200

Table 1
Flow parameters for Billy et al.'s experiments

Case	r_0 (cm)	Q (μl/min)	Re	Pe	Kinetic parameters			
					Apparent		Intrinsic	
					k_m (nM)	w_{max} [fmole/(s cm^2)]	k_m (nM)	w_{max} [fmole/(s cm^2)]
1	0.0325	30	0.42	4897.8	6.6	0.805	1.3	0.7224
2	0.0145	440	13.79	160 950	3.9	1.215	2.8	1.197

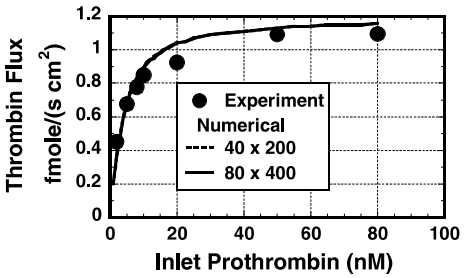

Fig. 2. Effect of spatial grids on the average thrombin flux.

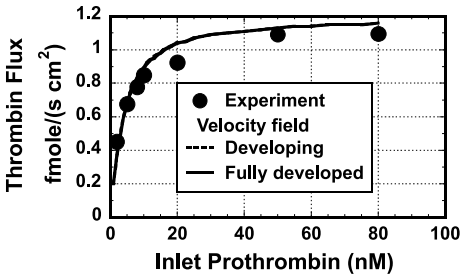

Fig. 3. Effect of developing and fully developed flow fields on the average thrombin flux.

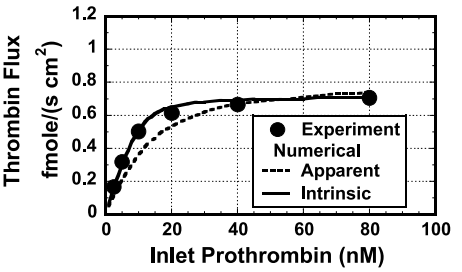

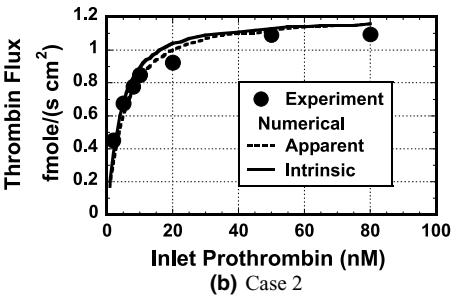

Fig. 4. Comparisons of thrombin production rate obtained from numerical computations and experimental data for two volumetric flow rates: (a) 30 μl/min, (b) 440 μl/min.

control volumes are used in all subsequence computations. The flow field is allowed to develop in this spatial grid study. It will be shown (see Fig. 3) that the flow field can be assumed to be fully developed without affecting the present conclusion.

Fig. 3 shows the comparison between fully developed and developing flow fields for case 2. Similar to the grid sensitivity study, the predicted average thrombin productions are identical. Although not shown, both the spatial grid resolution and velocity field studies on the low volumetric flow rate case (case 1) show the same conclusion. As a result, all subsequent computations are carried out using 40×200 control volumes and fully developed velocity field.

Fig. 4 shows the comparisons between the computed and experimental results for both flow rates. Both apparent and intrinsic kinetic parameters produce reasonable solutions compared to the experimental data. At lower flow rates, solutions obtained using the intrinsic parameters match the published experimental results better. At higher flow rates, both apparent and intrinsic parameters produce similar results. The present numerical results are tabulated in Table 2.

3.2. Problem 2

3.2.1. Problem description

The experiment was presented by Gemmell et al. [3]. Similar to the previous problem, it consists of flow inside a circular tube. The length of the tube was kept at 12.8 cm for all cases. The tube radius was 0.0135 cm. The important parameters are summarized in Table 3. The ratio between the density and viscosity is $\rho/\mu = 265.2$ s/cm^2. The diffusion coefficient of Factor X is $D_s = 5.0 \times 10^{-7}$ cm^2/s. The schematic of the problem is shown in Fig. 1(a).

3.2.2. Discussions of results

The effects of spatial grids and developing velocity field are examined. It was observed that the fully developed velocity profile could be used without changing the solutions. Similarly, grid independent solutions have been obtained using 40×200 control volumes in the radial and axial directions, respectively. As a result, the computational grids used in the previous study are also employed here. Fig. 5 shows the comparisons between the computed results and the available experimental data for different shear rates and inlet Factor X concentrations. It can be seen that the computational results match the experimental data quite well.

3.3. Problem 3

3.3.1. Problem description

Hall et al. [4,6] conducted experimental measurements and numerical simulations of the production of Factor Xa in parallel channel. Transient production of Factor Xa are presented for six shear rates, namely, 10, 20, 40, 80, 320, and 1280 s^{-1}. The steady-state Factor

Table 2
Predicted thrombin flux

C_{in} (nM)	Thrombin flux [fmole/(s cm^2)]			
	30 μl/min		440 μl/min	
	Apparent	Intrinsic	Apparent	Intrinsic
1	0.05	0.060	0.17	0.20
2	0.09	0.13	0.31	0.37
3	0.13	0.19	0.43	0.49
4	0.17	0.24	0.52	0.60
5	0.21	0.30	0.60	0.67
6	0.24	0.35	0.66	0.74
7	0.27	0.39	0.71	0.79
8	0.30	0.44	0.76	0.83
9	0.33	0.47	0.79	0.86
10	0.36	0.51	0.83	0.89
11	0.38	0.53	0.85	0.92
12	0.41	0.56	0.88	0.94
13	0.43	0.58	0.90	0.95
14	0.45	0.59	0.92	0.97
15	0.46	0.61	0.94	0.98
16	0.48	0.62	0.95	1.00
17	0.50	0.63	0.96	1.01
18	0.51	0.64	0.98	1.02
19	0.52	0.64	0.99	1.03
20	0.53	0.65	1.00	1.04
22	0.56	0.66	1.02	1.05
25	0.58	0.67	1.04	1.07
27	0.60	0.68	1.05	1.08
30	0.62	0.68	1.07	1.09
35	0.65	0.69	1.09	1.10
40	0.67	0.69	1.10	1.11
45	0.68	0.70	1.10	1.12
50	0.69	0.70	1.12	1.13
55	0.70	0.70	1.13	1.14
60	0.71	0.70	1.14	1.14
65	0.72	0.71	1.14	1.15
70	0.73	0.71	1.15	1.15
75	0.73	0.71	1.15	1.15
80	0.74	0.71	1.16	1.16

Table 3
Flow parameters for Gir et al.'s experiments

γ (1/s)	u_{in} (cm/s)	Re	Pe	k_m (nM)	w_{max} [fmole/(s cm^2)]
100	0.338	1.208	9040.2	140	42.133
300	1.013	3.625	27120.5	89.6	48.617
600	2.025	7.250	54241.1	107.8	55.1
1200	4.05	14.500	108482.1	92.4	52.783
1800	6.075	21.750	162723.2	39.2	49.3
2400	8.1	29.000	216964.3	15.4	48.617

Xa fluxes are predicted for selected shear rates. The length of the channel was kept at 4.5 cm for all cases. The height of the channel was 0.01 cm. The important parameters are summarized in Table 4. The ratio between the density and viscosity is $\rho/\mu = 1000$ s/cm^2.

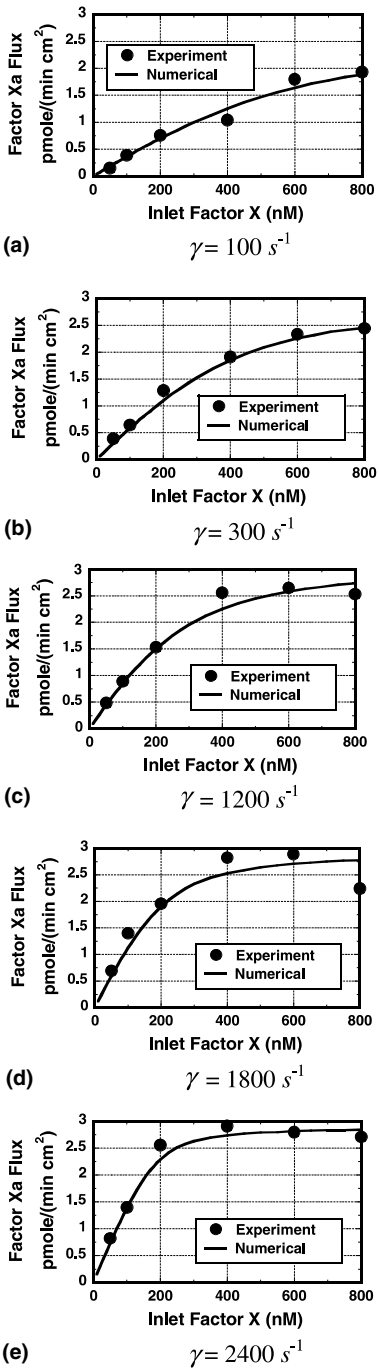

Fig. 5. Comparisons of Factor Xa production rate obtained from numerical computations and experimental data for five volumetric flow rates.

The diffusion coefficient of Factor X is $D_s = 5.0 \times 10^{-7}$ cm^2/s. The inlet concentration of Factor X was set to 100 nM. The schematic of the problem is shown in Fig. 1(b).

Table 4
Flow parameters for Hall et al.'s experiments

γ (1/s)	u_{in} (cm/s)	Re	Pe	k_m (nM)	w_{max}[a] [fmole/(min cm^2)]
10	0.0167	0.167	333.333	36	
20	0.0333	0.333	666.667	36	124
80	0.1333	1.333	2666.67	36	200
320	0.5333	5.333	10666.7	36	
1280	2.1333	21.333	42666.7	36	792

[a] Ref. [6].

Table 5
Comparison of present predictions with Hall et al.'s data

γ (1/s)	w_{max} [fmole/(min cm^2)]	Hall et al.		Present numerical [fmole/(min cm^2)]
		Experiment [fmole/(min cm^2)]	Numerical [fmole/(min cm^2)]	
20	124	95±20	86	85.5
80	200	138±33	139	139
1280	792	593±34	533	532.6

Table 6
Comparison of present predictions with Hall et al.'s data

γ (1/s)	w_{max} [fmole/(min cm^2)]	Experiment [fmole/(min cm^2)]	Numerical [fmole/(min cm^2)]
10	100	69 ± 18	67.7
20	140	95 ± 20	95.6
80	200	138 ± 33	139
320	475	317 ± 44	320.6
1280	900	593 ± 34	596.4

3.3.2. Discussions of results

The effects of spatial grids and developing velocity field are also examined. Similar to the previous problems, it was observed that the fully developed velocity profile could be used without changing the solutions. Similarly, grid independent solutions have been obtained using 40×200 control volumes in the transverse and axial directions, respectively. This indicates that the solution procedure is quite robust. The value of k_m is set to 36 nM in all computations. Table 5 shows the comparisons between the present predictions with the experimental data and numerical solutions of Hall et al. The w_{max} values suggested by Hall et al. are used in these comparisons. It can be seen that the present predictions match the predictions of Hall et al. very well. The values of w_{max} are "optimized" and the results are shown in Table 6. Each shear rate simulation requires about five seconds of CPU time on a Pentium III 700 MHz personal computer.

4. Concluding remarks

A finite-volume method is used to model the formation of Factor Xa from Factor X, and the formation of thrombin from prothrombin. It is found that the average production rate is the same for both the fully developed flow and developing flow. Three sets of experiments are simulated and the results match the experimental data very well. Therefore, the classical Michaelis–Menten enzyme kinetics can be used to describe two important steps in the blood coagulation cascade once steady state has been reached. To show the robustness of the procedure, the same computational grid is used in all three simulations.

References

[1] G. Michal (Ed.), Biochemical Pathways: An Atlas of Biochemistry and Molecular Biology, Wiley, New York, 1998.
[2] D. Billy, H. Speijer, G. Willems, H.C. Hemker, T. Lindhout, Prothrombin activation by Prothrombinase in a tubular flow reactor, J. Biol. Chem. 270 (3) (1995) 1029–1034.
[3] C.H. Gemmell, Y. Nemerson, V.T. Turitto, Factors affecting the interaction of tissue factor/factor VII with factor X in a heterogeneous flow reactor, Thromb. Haemostasis 65 (1991) 139–143.

[4] C.L. Hall, M.B. Taubman, Y. Nemerson, V.T. Turitto, Factor Xa generation at the surface of cultured rat vascular smooth muscle cells in an in vitro flow system, J. Biomech. Eng. 120 (1998) 484–490.

[5] S. Gir, S.M. Slack, V.T. Turitto, A numerical analysis of factor X activation in the presence of tissue factor–factor VIIa complex in a flow reactor, Ann. Biomed. Eng. 24 (1996) 394–399.

[6] C.L. Hall, S.M. Slack, V.T. Turitto, A computational analysis of FXa generation by TF:FVIIa on the surface of rat vascular smooth muscle cells, Ann. Biomed. Eng. 26 (1998) 28–36.

[7] S.V. Patankar, Numerical Heat Transfer and Fluid Flow, Hemisphere, New York, 1980.